FLOW IMAGING IN CORE SAMPLES BY ELECTRICAL IMPEDANCE TOMOGRAPHY

J.J.A. van Weereld (1), M.A. Player (2), D.A.L. Collie (3), A.P. Watkins (3), D. Olsen (4)

(1) Geolink, Aberdeen (2) Department of Engineering, University of Aberdeen, Scotland
(3) Robertson Research International Ltd., Aberdeen (4) Geological Survey of Denmark and Greenland, Copenhagen, Denmark

ABSTRACT

3D Electrical Impedance Tomography (EIT) provides *in-situ*, steady or unsteady state, imaging of fluid distribution in core samples at reservoir pressures. Although spatial resolution is not able to match that obtained through x-ray CT or MRI, the technique provides an inexpensive, simple, practical and safe means of monitoring the resistivity distribution of reservoir fluids in a 38 mm core plug, in near real-time and in full 3D.

An array of 192 electrodes carried on a flexible printed circuit is wrapped around a core plug mounted in a Hassler or Hoek-type core holder. A fast bipolar current pulse allows a 4-wire type resistance measurement on all electrodes around the surface of the core sample. A data set is thus generated that embodies the 3D resistivity/conductivity profile of the whole sample as a transresistance matrix. Processing of these measurements reconstructs the full 3D internal resistivity distribution, and correspondingly the distribution of conducting fluids in the sample.

The iterative reconstruction algorithm utilises a Finite Element forward model, for the cylindrical core plug, comprising 1080 triangular prismatic linear Galerkin elements. Regularised Jacobian and Hessian matrices of the non-linear inverse problem are constructed, and inversion uses Levenberg-Marquardt and truncated-Newton algorithms, implemented in MATLAB.

The real-time capability of EIT data acquisition permits imaging and analysis of the two-phase saturation system, including flow-front monitoring, characterisation of the flow regime, the distribution of residual oil or water at the final stages of relative permeability tests, and capillary end effects. Initial laboratory tests demonstrate repeatability and reliability of results.

INTRODUCTION

Core analysis is concerned with the study of fluid-rock interactions in rock samples obtained from hydrocarbon reservoirs. The samples are usually in the shape of cylinders, with a nominal diameter of 38 mm and a length of 50 mm. The fluids involved in these studies are crude or synthetic oil, and brine. In various static and dynamic experiments the resistance of the sample is measured, and the resistivity calculated. This can in turn be related to fluid saturation [1].

back to contents

The two- or four-wire measurement is commonly made with a commercially available LCR bridge with sinusoidal excitation. Problems exist with obtaining a satisfactory contact between the sample and the measurement electrodes, especially for samples with low water saturation. The art involved in making the measurements involves the application of silver filter discs or brine wetted tissue as contact materials, and choosing a measurement frequency for minimum phase angle [2]. Nevertheless, if these problems can be controlled, the large difference in resistivity of the fluids involved suggests Electrical Impedance Tomography (EIT) as an ideal method for imaging fluid distribution in the sample.

In EIT generally, and specifically here Electrical Resistance Tomography, an image of resistivity (the specific resistance of the material, Ωm) throughout the volume of an object is reconstructed from measurements of resistance (two- or four-wire voltage/current ratios, Ω) taken at the surface. This generates a non-linear, ill-posed inverse problem, because the resistivity distribution in the sample itself modifies the flow of current, and the sensitivity to changes in resistivity depends strongly on position within the sample [3]. In this respect the method is more computationally demanding than x-ray tomography, where the inverse problem is essentially linear. We have adopted a well-known reconstruction method for EIT, which uses iterative least squares to minimise the difference between finite element (FE) estimates of resistance and the actual measurements [3, 4, 5]. However, a direct implementation is particularly computationally intensive, requiring some variation to give acceptable times for 3D reconstruction.

This paper describes our approaches to the measurement and algorithmic issues raised by EIT, and gives results for flow of oil and brine through sandstone samples. Derivation of the saturation distribution on a voxel (3D-pixel) by voxel basis should follow directly using pore structure information established from measurements on a fully water saturated sample, and from sample petrographic parameters and brine resistivity. We expect this to be the subject of further work.

RESISTANCE MEASUREMENT

Consider a core to which N electrodes are attached. An individual resistance value is obtained by connecting a current generator to one pair of electrodes, and measuring voltage between another pair, and a dataset for an EIT reconstruction will in principle consist of all such measurements. However these are not all independent and, taking account of reciprocity, the maximum number of independent measurements is $\frac{1}{2}N(N-1)$. To obtain 3D reconstructions, it is clear that electrodes should be spread fairly uniformly over the surface of the sample, and it is also clear that in principle the resolution should rise with the number of electrodes. We have used an array of 192 electrodes (8 rings of 24) placed on the circumference of the sample. This number is a compromise between resolution on one hand, and manufacturability of the electrode array and computing capacity for the reconstruction algorithm on the other.

Each electrode in contact with the brine forms an electrochemical interface, which is well understood [6]. In an electrical sense, the interface can be considered as a capacitor, C_d, usually referred to as the double layer capacitor, in parallel with a resistor R_e, the latter being not necessarily linear (figure 1). The values of R_e and C_d are dependent on electrode material, brine constituents, and applied potential. The electrode material determines whether the system is reversible (i.e. if the chemical reaction on the electrode by an electric current can be reversed by reversing the current), or irreversible. The latter is also referred to as a polarisable electrode. An example of the former is a silver-silver chloride electrode, an example of the latter gold or platinum. For a reversible electrode its behaviour is predominantly governed by R_e, for the polarisable electrode by C_d. A frequent method for dealing with this situation is to use AC measurement, as in a single resistance determination. However this normally requires digitising the sinewave response over a number of cycles, and compensating for the phase-shifts resulting from the various capacitances. We have instead used a "bipolar DC pulse" technique. Using this measurement method in combination with suitable multiplexing and control circuitry, a data acquisition system for impedance tomography has been successfully designed.

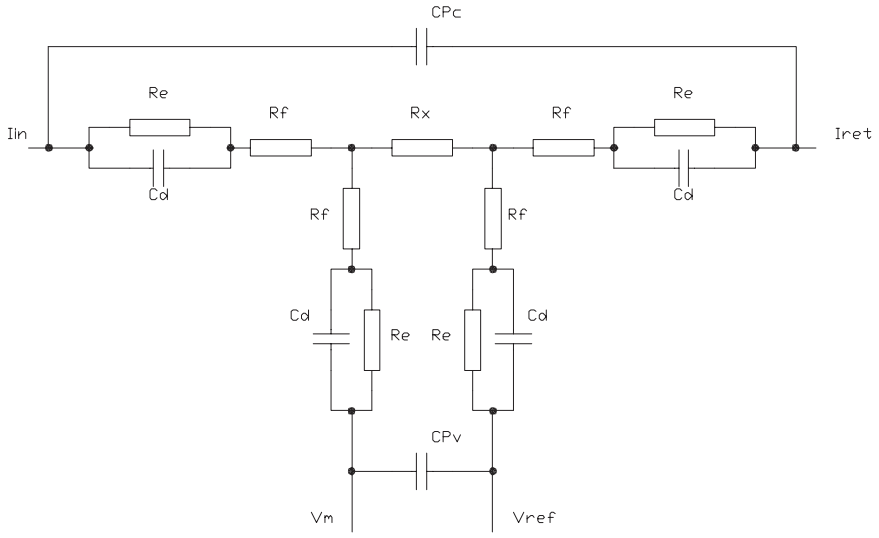

Figure 1. Electrode model.

For a four-wire DC measurement a stable current will have to be established in the subject of interest, for the time it takes to make a voltage measurement to the required precision. During this time no irreversible process should take place: i.e. when the electrodes are of a polarisable kind, the voltage to which the double layer capacitance is charged by the measurement current I, should remain below the voltage at which an electrochemical reaction will take place. This determines the maximum value of the current pulse duration t (figure 2). The total net charge transported through the solution during the measurement should be zero to avoid permanent changes to its properties. It follows that a pulse of reversed current will have to be applied with an equal product It. The impedance of the voltage measurement circuitry will be generally much larger than the electrode equivalent

parallel resistance R_e, and will therefore correctly measure the voltage generated by the constant current over the unknown resistance R_x. The minimum duration of the current pulse is determined by (i) the parallel parasitic capacitance C_{Pc} in the current electrode circuitry in conjunction with the measurement current, (ii) the parallel parasitic capacitance C_{Pv} in the voltage measurement circuitry in relation to the resistance of the medium R_x and R_f, and to the aperture time of the A to D (analog-to-digital) converter used in the measurement circuit.

The required application of a bipolar current pulse has an added benefit. The potential difference between electrode and solution (brine), which exists in every electrochemical interface, may not be the same for practical electrodes. This electrode offset V_{os} may be caused by concentration fluctuations in the solution, or property variations of the electrode material. If a voltage measurement is made during both positive and negative current pulses, and the absolute values of the currents are the same, this offset voltage can be calculated and removed (figure 2). The same is true for offset voltages in the input circuitry for the voltage measurement. Two-wire bipolar pulse conductivity measurements have previously been proposed for the measurement of chemical reaction rates [7, 8, 9], in which offset compensation was implemented in hardware.

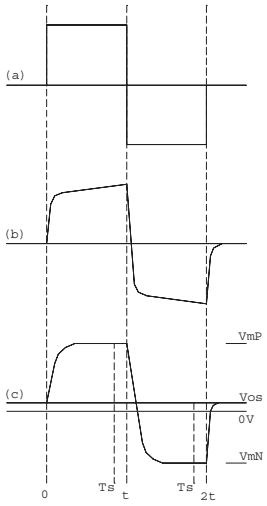

Figure 2. Waveforms for the “bipolar DC pulse” method.

The task of attaching 192 electrodes to the cylindrical surface of the sample has been made relatively simple, by depositing the electrodes on a flexible printed circuit board (figure 3), which is then wrapped around the sample. The geometrical position of the electrodes on the flexible circuit is fixed, which restricts the size of the sample to a length of 50 mm, and a diameter of 38 mm. The electrodes are electro-plated with the required electrode metal. The flexible circuit is a disposable item.

The assembly can be used in a Hassler or Hoek-type core holder (figure 4), as the part of the flexible circuit carrying the connections to the electrodes is brought out between the confining sleeve [C] and the “fixed” platen [E]. Application of confining pressure [Q]

ensures the electrodes are firmly in contact with the sample [D]. Proprietary construction of the flexible printed circuit prevents any leakage between electrodes, or between circuit and platen where it exits the cell. The flexible circuit attaches to connectors [K] which are an integral part of the cell electronics (multiplexer), mounted on support plate [M]. The platens are manufactured from PEEK (poly aryl ether ether ketone) for electrical insulation.

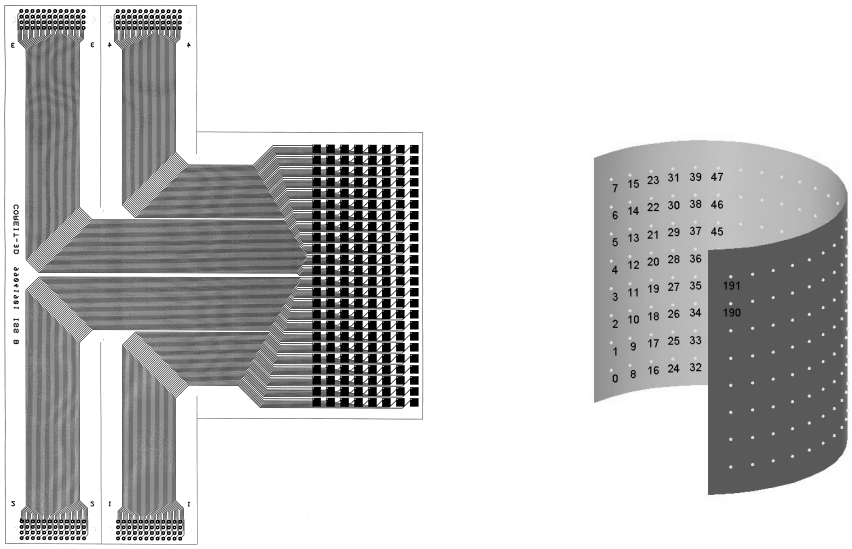

(a) (b)

Figure 3. Flexible electrode array. (a) Layout of flexible printed circuit board: 8×24 electrode array on the right, four connector pads at top and bottom. (b) Indication of electrode layout and numbering when applied to core surface.

Electrically the system consists of three main components. All control circuitry is accomodated on a single PC ISA bus card. Control signals are optically coupled to the analog electronics and to the multiplexer, to prevent ground induced noise. The analog electronics comprises current pulse generator and voltage measurement circuitry, and is housed with its own linear power supply in a separate screened enclosure. The multiplexer consists of electronic switches to select current and voltage electrodes and is mounted directly on the core holder, to keep the (high impedance) voltage path as short as possible.

The resolution for the voltage measurement is 16 bits. Depending on current levels and resistance values, tests on a single "dummy sample" simulating the circuit of figure 1 show standard deviations of between 1 and 4 LSB's. It is obviously more difficult to characterise circuit performance on real samples, but comparisons between datasets suggest a similar level of variation. A limit on the speed of the data acquisition is imposed by the input capacitance of the current switch. If the sample has a relatively high resistivity, the use of low currents is required to remain in the measurement range of the A to D converter. The input capacitance of the current switch is approximately 3.5 nF, the main part of which is

formed by the 192 current multiplexer switches. For worst-case scenarios the time required to acquire a full data set of 192×192 measurements is approximately 19 s ($t = 256$ µs). For larger injection currents the pulse duration t can be chosen progressively smaller, for instance, for currents > 1 mA the time required for a measurement reduces to 32 µs, and the time to acquire a full data set to approximately 2.5 s.

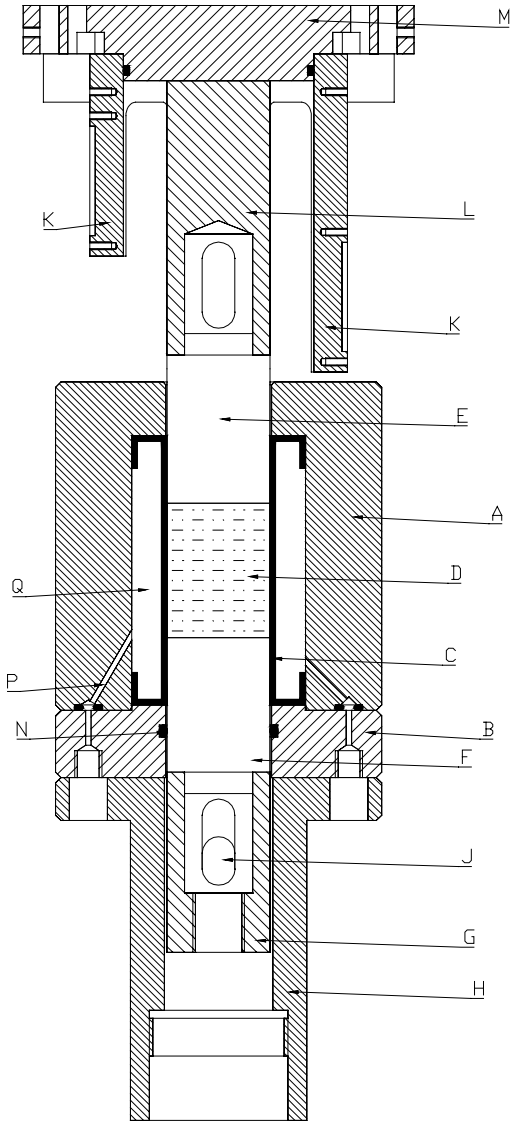

Figure 4. Cross-section of core holder.

IMAGE RECONSTRUCTION

The EIT hardware is configured to capture its full data set of 192×192 measurements using a variation of the well-known "diagonal" scheme, in which essentially a single electrode is chosen as current "dump", and all other electrodes are used in turn as current

sources. We used a scheme that numbers neighbouring electrodes along the axial direction consecutively, choosing each axial row in turn and numbering always in the same direction (figure 3(b)). Current dump and voltage reference are then selected close together, usually on electrode ring 3 (approximately half way along the sample). Injection at all 192 electrodes follows, with the measurement of the required 192 voltage measurements for each injection. This pattern is repeated three more times for the reference pair located similarly but one quarter, one half and three quarters around the sample. Additionally, at least one identical data set is captured immediately and compared to provide an assessment of the reliability of the data.

The full data set is then recast as a transresistance matrix R_T, which represents the data independently of the particular measurement scheme. We use a formulation for which the voltage variables V are branch voltages between adjacent electrodes, and the current variables I are corresponding loop currents. Matrix elements represent the ratios of these values for particular electrode pairs:

$$V = R_T I \tag{1}$$

This formulation has the advantage that most elements can be determined using only four-wire voltage and current measurements. Since R is symmetrical, this process reduces the volume of data passed to the reconstruction algorithm.

A well-known reconstruction method uses iterative least squares to minimise the difference between Finite Element (FE) estimates of resistance and the actual measurements [3, 4, 5]. The Levenberg-Marquardt algorithm [10] has been found particularly useful. It is a full Newton approach, where each iteration step requires calculation and inversion of the second derivative of the cost function (Hessian matrix). Tikhonov regularisation, adding a quadratic smoothness constraint to the cost function, improves conditioning of the problem, although it may bias the final image [5, 11]. The update equation of the regularised Levenberg-Marquardt method is [11]:

$$\left(J_k{}^T J_k + \alpha R + \varepsilon I\right)\Delta\rho = J_k{}^T \left(R_{EIT} - R_{FE}(\rho_k)\right) - \alpha R \rho_k \,. \tag{2}$$

Here ρ_k is the vector of resistivity values, at iteration k, and $\Delta\rho$ the resistivity update. R_{EIT} and R_{FE} are the measured and estimated transresistance matrices (reordered as vectors). The Jacobian matrix J_k expresses the derivative of the vector V_{FE} with respect to ρ_k. R is the regularisation matrix. Parameters α and ε control, respectively, levels of Tikhonov and of Levenberg-Marquardt regularisation. In implementing equation 2, the major computational bottleneck is calculation of the product $J_k{}^T J_k$ [4, 10]. This is particularly important for true 3D geometry. To retain the basic, highly effective, structure of the Levenberg-Marquardt method, but to avoid a full matrix multiply, we have used a truncated-Newton (TN) algorithm in which solution of equation 2 is performed using the

preconditioned conjugate gradient (PCG) algorithm [12]. The update at iteration *i* involves the Hessian matrix *H* only through the expression [13]

$$q_i = J_k{}^T (J_k p_i) + (\alpha R + \varepsilon I) p_i \qquad (3)$$

the significance of which is that only matrix-vector multiplications are required. The overall cost of the solution then depends on the rate of PCG convergence. Convergence is improved by preconditioning, which in effect multiplies *H* by an approximation to its inverse. If elements of J_k with low absolute value are truncated to zero, the resulting sparse approximation $J_{(S)k}$ provides a useful preconditioner:

$$M = J_{(S)k}{}^T J_{(S)k} + \alpha R + \varepsilon I \qquad (4)$$

at substantially lower cost than for the full product *H*. Behaviour of the outer Levenberg-Marquardt loop of this algorithm is controlled, as usual, by parameters α and ε, while the inner PCG loop is controlled by parameters that set the sparsity of $J_{(S)k}$ and the tolerance on PCG convergence. In practice, sparsity can be set so that adequate PCG convergence is obtained with around 10 iterations, and the time taken for the PCG solution is roughly equal to the time taken to form (and factorise) *M*.

This algorithm requires an FE model to solve the forward problem, and to generate the Jacobian *J*. Upright triangular prismatic elements are well suited geometrically to meshing of the cylindrical core, and also yield a relatively straightforward analytical form for the 6-node linear Galerkin local admittance matrix. (We have verified our own analytical formulation by comparison with Pinheiro *et al.* [14].) However, decomposing each prism into 3 tetrahedra, and averaging over the 6 possible decompositions, is found to give better accuracy. The 3D solutions generated by this forward model are closer to actual measured results than those from 2D calculations as commonly used in EIT. This is not surprising in view of the highly artificial assumption, inherent in the 2D models, that current flow is restricted to planes [5, 10]. Delaunay triangulation is used to generate the FE mesh.

Tests on the TN reconstruction scheme indicate acceleration by a factor of about 9, compared with direct multiplication to form the Hessian. For an FE mesh of 1080 elements (9 rings of 120 elements, equivalent to a spatial resolution of approximately 4×4×4 mm^3) the time per iteration at optimum parameter settings is about 134 seconds on a 450MHz PC, and convergence to a final image typically requires 4 to 6 iterations. Accuracy of recovered resistivity in simulations, using realistic values of resistivity contrast, is generally within 5% over regions of fairly constant resistivity. Obviously, the local accuracy falls in regions of high resistivity gradient, where the FE mesh cannot represent the resistivity correctly. However, there may also appear local anomalies due to operation of the algorithm. Modifying regularisation to a mixture of quadratic constraints on resistivity and conductivity is fairly effective at controlling these. On the other hand, accuracy rises for more uniform samples.

RESULTS AND DISCUSSION

A view of the complete system, assembled on the sample holder, is shown in figure 5.

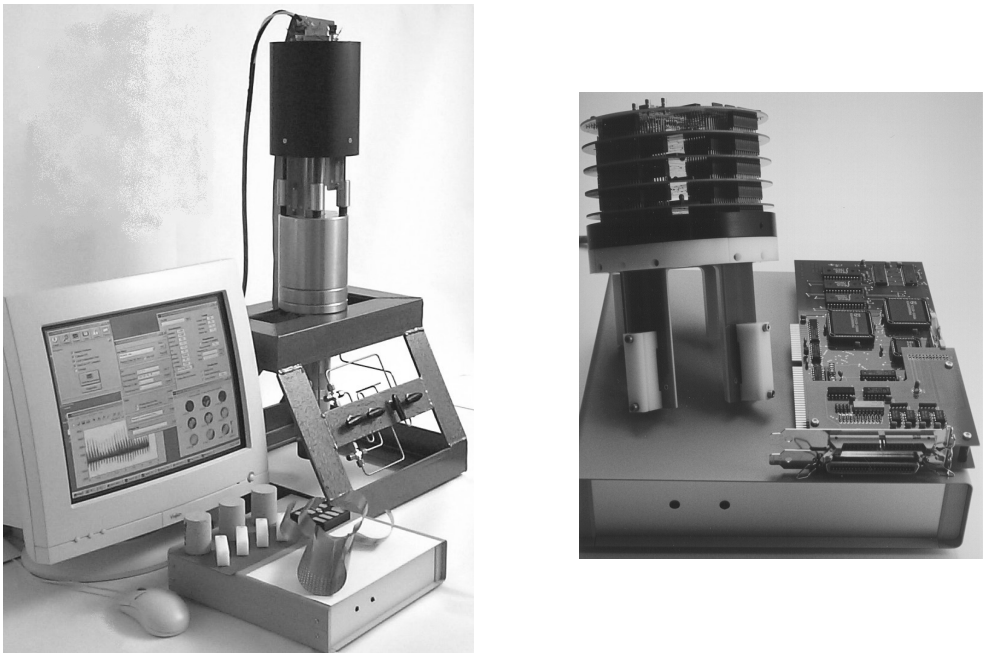

(a) (b)

Figure 5. (a) Complete EIT system. Note electronics housing for multiplexers mounted above the Hoek-type core holder. Analog electronics are housed in the case in front of the monitor. A flexible printed circuit electrode array is shown on top of the case.
(b) Multiplexer assembly and ISA interface card.

This is the set-up used for flow tests on cores: we have also carried out tests using a brine cell into which insulating "phantoms" can be inserted. Figure 6 shows results from the brine cell phantom, consisting of two eccentric cylinders. This indicates generally good fidelity of the reconstruction, within the restriction imposed by the relatively coarse resolution. The "rounding-off" apparent in the conductivity isosurface is due as much to the coarse meshing as to smoothing from the Tikhonov regularisation.

For work on cores, we have used Bentheim sandstone, a medium grained, very homogeneous, and clean sandstone, light brownish in colour, and with an absence of visible oriented structures. It comes from an outcrop in Germany. Figure 7 shows three reconstructions from a sequence in which brine was flowed into a core initially oil-saturated, but with irreducible brine. Development of a conical flow front is apparent.

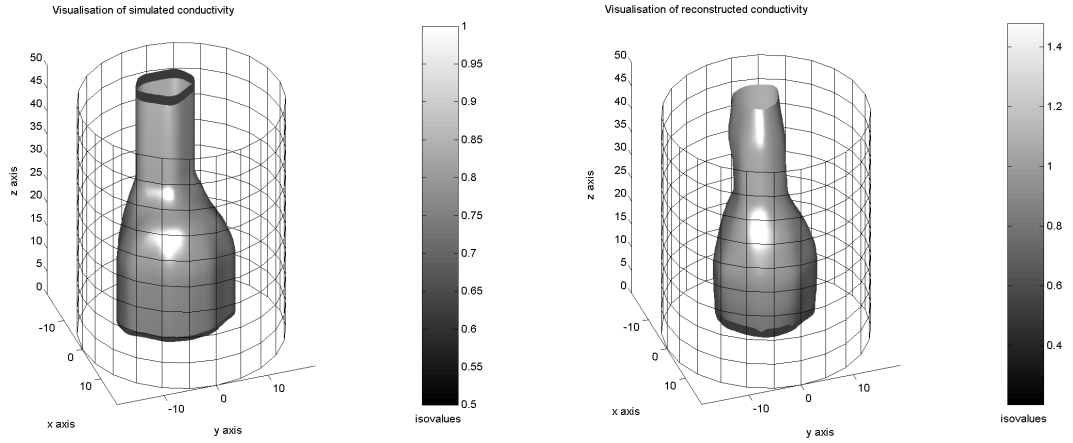

(a) (b)

Figure 6. Imaging of brine cell phantom. (a) Original phantom visualised using the same grid as reconstruction. (b) Reconstruction.

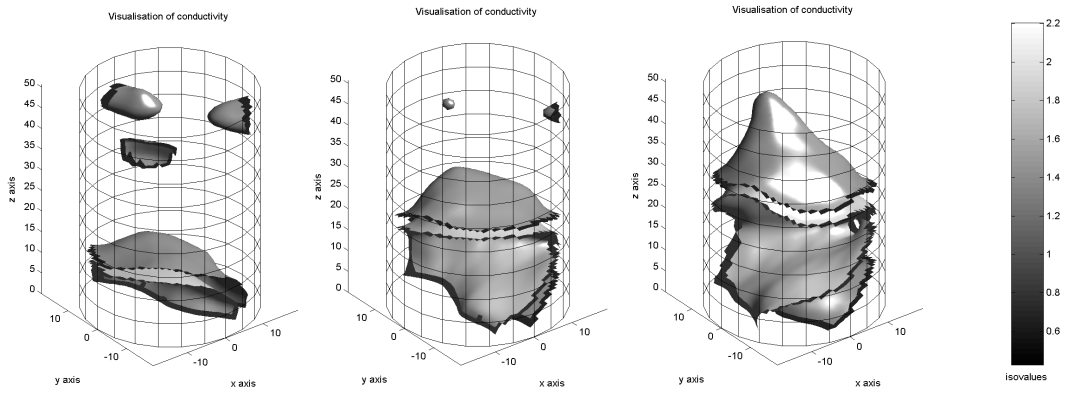

(a) (b) (c)

Figure 7. Sequence of images of brine flow in initially oil-saturated sample. Brine flow at 1 cm^3min^{-1}, 14 cm^3 pore volume, initially 5 cm^3 irreducible brine, 9 cm^3 oil. (a) After 1 min 45 sec. (b) After 3 min 19sec. (c) After 4 min 56 sec. Linear units are mm; isovalues are arbitrary conductivity units.

There are some anomalies visible in these images: the reasons for these are not always clear, but the most likely causes are imperfections in the data itself arising from poor contact and surface leakage, and inaccuracies in matching the geometry of the FE model to that of the core, particularly near the ends of the sample. Our experience is that care is required to collect a good-quality data set. Data can be degraded by instability in the active current dump circuitry, but this is minimised by suitable choices of dump and reference electrodes. Currents must be selected to avoid excessive overload of the A to D converters on two-wire measurements: even though these values are discarded, there is an effect on neighbouring measurements, not so far fully explained. Even with these precautions, data sets may show anomalous values for voltage measurements on electrodes close to current

injection points, and these may have to be manually removed using a data pre-processing facility in the acquisition software.

So far, we have not been able to complete a full quantitative comparison with other methods. However, we can draw the following conclusions:

- Data for a complete 3D EIT "snapshot" can be acquired, using the bipolar DC pulse technique, in less than 1 minute, including duplicate datasets.
- A 3D reconstruction can typically be completed in under 10 minutes, for a resolution equivalent to a $4\times4\times4$ mm^3 voxel over a standard 38 mm diameter by 50 mm core. This is approximately 9 times faster than for unmodifed Levenberg-Marquardt reconstruction, with no loss of accuracy.
- Repeatability of the resistance measurements, on a simulated electrode structure, is within a few LSB's (on a 16-bit A to D converter), and is generally similar on real samples.
- Accuracy of the reconstruction algorithm is typically 5% over regions of uniform resistivity, though it is subject to reduced accuracy both in rapidly varying regions and through the appearance of localised anomalies in some circumstances. This accuracy is much enhanced compared with a 2D EIT reconstruction using "slices", as the full 3D current flow is taken properly into account.

Further work is needed to convert resistivity images to saturation, to validate results against other methods, and also to improve the known imperfections in data acquisition and reconstruction. For acquisition, these include tracing and eradicating remaining causes of irreproducible measurements. For reconstruction, additional work on algorithm design and re-coding should further improve speed, but the main challenges are resolution and accuracy. There is considerable scope for improvement in the FE forward model, by use of higher-order elements and possibly adaptive meshing, and improved spatial representation of the resistivity.

The authors gratefully acknowledge the financial support of the European Commission through Contract JOF3-CT97-0032 under the Non Nuclear Energy Programme (JOULE III), and the financial support and encouragement of Shell, Amerada Hess and Enterprise Oil. We also thank the University of Aberdeen, Robertson Research International and the Geological Survey of Denmark and Greenland (GEUS) for their support of the project.

REFERENCES

1 Ohirhian P.U., "An explicit form of the Waxman-Smits equation for shaly sands," *The Log Analyst*, (1998) **39**, 3, 54-57.

2 Worthington P.F., Evans R.J., Klein J.D., Walls J.D. and White G., "SCA guidelines for sample preparation and porosity measurement of electrical resistivity samples; Part III – The mechanics of electrical resistivity measurements on rock samples," *The Log Analyst*, (1990) **31**, 2, 64-67.

3 Yorkey T.J., Webster J.G. and Tompkins W.J., "Comparing reconstruction algorithms for electrical impedance tomography," *IEEE Trans.*, (1987) **BME-34**, 11, 843-852.
4 Dickin F. and Wang M., "Electrical resistance tomography for process applications," *Meas. Sci. Technol.*, (1996) **7**, 3, 247-260.
5 Player M.A., van Weereld J., Hutchinson J.M.S., Allen A.R. and Shang L., "An electrical impedance tomography algorithm with well-defined spectral properties," *Meas. Sci. Technol.*, (1999) **10**, 3, L9-L14.
6 Bockris J.O. and Khan S.U.M., *Surface Electrochemistry, A Molecular Level Approach*, Plenum Publishers, New York 1993.
7 Johnson D.E. and Enke C.G., "Bipolar Pulse Technique for Fast Conductance Measurement," Analytical Chemistry, (1970) **42**, 3, 329-335.
8 Daum P.H. and Nelson D.F., "Bipolar Current Method for Determination of Solution Resistance," *Analytical Chemistry*, (1973) **45**, 3, 463-470.
9 Caserta K.J., Holler F.J., Crouch S.R. and Enke C.G., "Computer controlled bipolar pulse conductivity system for applications in chemical rate determinations," *Analytical Chemistry*, (1978) **50**, 11, 1534-1541.
10 Press W.H., Flannery B.P., Teukolsky S.A. and Vetterling W.T., *Numerical Recipes in C*, Cambridge University Press, Cambridge 1993.
11 Binley A., Shaw B. and Henry-Poulter S., "Flow pathways in porous media: electrical resistance tomography and dye staining image verification," *Meas. Sci. Technol.*, (1996) **7**, 3, 384-390.
12 Schlick T. and Fogelson A., "TNPACK - A truncated Newton minimization package for large-scale problems. I. Algorithm and usage," *ACM Trans. on Mathematical Software*, (1992) **18**, 1, 46-70.
13 Barrett R., Berry M., Chan T.F., Demmel J., Donato J., Dongarra J., Eijkhout V., Pozo R., Romine C. and van der Horst H., *Templates for the Solution of Linear Systems: Building Blocks for Iterative Methods*, SIAM, Philadelphia 1993.
14 Pinheiro P.A.T., Dickin F.J. and James A.E., "Analytical stiffness matrix for the first and second order upright triangular prismatic elements" *Commun. Numer. Meth. Eng.*, (1997) **13**, 6, 467-473.

back to contents